Targeting cells with single vectors using multiple-feature Boolean logic

Lief E Fenno[1,2,13], Joanna Mattis[1,2,13], Charu Ramakrishnan[2,13], Minsuk Hyun[2], Soo Yeun Lee[2,3], Miao He[4], Jason Tucciarone[4,5], Aslihan Selimbeyoglu[1], Andre Berndt[2], Logan Grosenick[1–3], Kelly A Zalocusky[1,3], Hannah Bernstein[6], Haley Swanson[3], Chelsey Perry[3], Ilka Diester[2,7], Frederick M Boyce[8], Caroline E Bass[9], Rachael Neve[10], Z Josh Huang[4] & Karl Deisseroth[2,3,11,12]

Precisely defining the roles of specific cell types is an intriguing frontier in the study of intact biological systems and has stimulated the rapid development of genetically encoded tools for observation and control. However, targeting these tools with adequate specificity remains challenging: most cell types are best defined by the intersection of two or more features such as active promoter elements, location and connectivity. Here we have combined engineered introns with specific recombinases to achieve expression of genetically encoded tools that is conditional upon multiple cell-type features, using Boolean logical operations all governed by a single versatile vector. We used this approach to target intersectionally specified populations of inhibitory interneurons in mammalian hippocampus and neurons of the ventral tegmental area defined by both genetic and wiring properties. This flexible and modular approach may expand the application of genetically encoded interventional and observational tools for intact-systems biology.

Understanding how defined cell types contribute to organism function is a central goal in biology and an acute challenge in neuroscience[1]. Recent development of optically modulated, genetically encoded tools for testing necessity and sufficiency of precise activity patterns[2,3] has enabled the causal linkage of neuronal activity to circuit dynamics and behavior, but these tools are only as good as their targetability within intact systems. Cell types[4] defined by gene expression pattern are targetable via either transgenic or viral approaches. Although genetically specific, the transgenic approach (inserting genes into defined loci to recapitulate native expression patterns) requires a new animal strain to be generated for each tool. In contrast, viruses are rapidly adaptable, with flexibility in tool payload and injection location. However, suitable promoter fragments (to drive expression of genetically encoded tools) must be short, strong and specific; the viral capsid determines packaging efficiency and limits this strategy[3]. Recent approaches have combined the versatility of viral intervention with fuller genetic specificity conferred by the native chromosomal environment by pairing recombinase-dependent viruses with recombinase-expressing animal lines[5–10].

Although these approaches are elegant, they define cell types by only a single feature. Moreover, cells identical by one marker may serve different or even oppositional roles in physiology or behavior. Therefore, there is strong motivation to enable cell-type definition by multiple features, including multiple genetic and wiring features. A versatile viral system for defining cell types on the basis of multiple features[4] with only a single nontoxic virus (such as adeno-associated virus (AAV) or lentivirus) would powerfully enhance opportunities arising from development of control and observational tools. Cell targeting based on multiple genetic factors generally requires crossing transgenic animals expressing multiple recombinases with animals that express a gene only after recombinase-dependent excision of multiple STOP cassettes[11]. This method has yielded insights into development but is less scalable and flexible than a viral approach, and it is further complicated by transient developmental promoter activity (triggering expression of recombinases), potentially leading to tool expression in off-target adult cell populations. Viral delivery in the adult would solve this temporal dilemma but is limited by viral payload limits[3] and the large size of STOP cassettes. Elegant approaches to logical gene expression using serine integrases have been described *in vitro*[12] but do not use recombinases typically built into transgenic mammals, and promoter manipulation strategies used in this approach can be 'leaky' *in vivo*, as we show here. Another approach splits proteins into two pieces, which are separately expressed; functionality results in only the cells that express both pieces. Though some function

[1]Department of Neuroscience, Stanford University, Stanford, California, USA. [2]Department of Bioengineering, Stanford University, Stanford, California, USA. [3]CNC Program, Stanford University, Stanford, California, USA. [4]Cold Spring Harbor Laboratory, Cold Spring Harbor, New York, USA. [5]Program in Neuroscience, Stony Brook University, Stony Brook, New York, USA. [6]Department of Neuroscience and Physiology, New York University School of Medicine, New York, New York, USA. [7]Ernst Struengmann Institute for Neuroscience, Frankfurt, Germany. [8]Department of Neurology, Massachusetts General Hospital, Cambridge, Massachusetts, USA. [9]Department of Pharmacology and Toxicology, School of Medicine and Biomedical Sciences, University at Buffalo, Buffalo, New York, USA. [10]Department of Brain and Cognitive Sciences, Massachusetts Institute of Technology, Cambridge, Massachusetts, USA. [11]Department of Psychiatry and Behavioral Sciences, Stanford University, Stanford, California, USA. [12]Howard Hughes Medical Institute, Stanford University, Stanford, California, USA. [13]These authors contributed equally to this work. Correspondence should be addressed to K.D. (deissero@stanford.edu).

RECEIVED 3 JANUARY; ACCEPTED 1 MAY; PUBLISHED ONLINE 8 JUNE 2014; DOI:10.1038/NMETH.2996

is generated with bacteriorhodopsin[13], channelrhodopsins are poorly expressed this way[14]. More importantly, construction of such an effector protein–specific targeting approach may not be rapidly adaptable to new tools.

Here we have created a versatile single-AAV system for selective expression that is conditional upon multiple cell-type features using Boolean logical operations. We validated the specificity and potency of the system (which involves custom-modified intronic sequences and diverse recombinases) by expressing opsins and fluorescent proteins both *in vitro* and *in vivo* within populations defined either positively or negatively by multiple genetic or wiring features. Designed for use with broadly available tools, this system is termed INTRSECT, for 'intronic recombinase sites enabling combinatorial targeting'.

RESULTS

Diversifying the single recombinase–dependent AAVs

We first sought to expand the 'double-floxed' inverted open reading frame (DIO) Cre-dependent expression system[5–8] by developing conditional-expression vectors dependent upon additional recombinases. We used a mouse-optimized version of Flp[15] that has been applied extensively in *Drosophila*[4], and we synthesized a human codon–optimized version of phage-derived Dre[16]. Cre, Flp and Dre recognize short palindromic sequences (*lox*, *FRT* and *rox* sites, respectively) that share a standard structure conferring both identity (sites with different palindromic spacer sequences cannot recombine) and directionality (sequence between two sites in the same direction is excised; sequence between sites in opposite directions is inverted; **Fig. 1a**). The DIO strategy uses both excision and inversion[5–8]. The targeted gene is initially antisense relative to the promoter, thereby preventing functional transcription. This inverted sequence is flanked by two pairs of incompatible recognition sites (for example, *loxP* and *lox2722*); two successive recombination events lock the targeted gene into the forward orientation (**Fig. 1b**). To create Flp- and Dre-dependent DIO systems (fDIO and dDIO), we used two *FRT* sites (*FRT* and *F5*; ref. 17), and because only one *rox* site was known, we created a novel site (*rox2*) by modifying the *rox*[16] spacer (**Fig. 1a**).

We investigated functionality and specificity of these DIO systems *in vitro* using channelrhodopsin (ChR2)-EYFP. HEK293 cells were transfected with each DIO alone, and also with each recombinase, and analyzed for fluorophore expression using flow cytometry (**Fig. 1c**,**d**). To quantify the results, we assessed whether the data were better fit by a single curve (indicating a uniform population of $EYFP^-$ cells) or by multiple curves (indicating mixed $EYFP^+$ and $EYFP^-$ cells; see Online Methods). All DIOs in isolation had expression levels comparable to that of the negative control (92–98% of random statistical subsamples of the data were fit by a single curve; Online Methods). When cotransfected with the correct recombinase, all DIOs had robust expression (99–100% of samples were fit by multiple curves; **Fig. 1d**). Notably, Cre and Dre exhibited cross-reactivity (78–92% of cDIO + Dre samples and 100% of dDIO + Cre samples were fit by multiple curves; **Fig. 1c**,**d**), whereas Flp and fDIO were independent of cDIO/dDIO and Cre/Dre, respectively (96–100% of samples were fit with a single curve).

To test *in vivo* functionality, we co-injected viruses encoding each DIO-ChR2-EYFP and each recombinase into mouse hippocampus (**Fig. 1e**). All DIOs had virtually no leak in isolation and had strong expression with the correct recombinase (**Fig. 1f**,**g**). Cross-activation was observed *in vivo* between dDIO-ChR2-EYFP and Cre (**Supplementary Fig. 1**) but not between Dre and cDIO-ChR2-EYFP. ChR2 stimulation *in vivo* evoked strong activity in all cases (**Fig. 1h**).

Development of a Cre- AND Flp-dependent construct

With the goal of targeting based on multiple features, we first paired Cre and Flp (chosen for the lack of detectable cross-reactivity and for increasingly available driver lines) to independently control relative directionality of the promoter and open reading frame (ORF; **Supplementary Fig. 2** and ref. 12), but we observed inappropriate expression *in vivo*. The second strategy used nested recombinases to manipulate separate domains of the ORF (**Supplementary Fig. 3**), but this suffered from low expression.

Next we considered that introns, present in DNA but excised during mRNA processing at conserved exon-intron boundary sequences[18,19], could allow for insertion of recombinase machinery directly into the gene without affecting the protein product. We first tested whether introns introduced into ChR2-EYFP would degrade protein functionality and whether insertion of recombinase recognition sites into introns would impair splicing. We identified intron insertion sites that naturally mimic exonic splice sequences[18,19] near the middle of each ORF, such that individual exons would be unlikely to encode functional protein. We inserted either of two introns: intron B from cytomegalovirus IE1 (ref. 20; 'intron 1', 112 bp) into ChR2 or intron 3 from mouse IgE (ref. 21; 'intron 2', 82 bp) into EYFP, with the introns either in native form or with an added *lox2722* ('+ *lox*') site within regions not likely to function in splicing. We also created a construct containing both introns (**Fig. 2a**).

HEK293 cells transfected with any of these constructs expressed EYFP, a result suggesting proper splicing. cDNAs synthesized by reverse transcription PCR (RT-PCR) from expressing cells and the source DNA were amplified by PCR using primer sets that spanned single introns (**Fig. 2b**) or both introns (**Supplementary Fig. 4a**). We noted variability in the size of the amplicon from the DNA template, whereas cDNA bands were uniform, further suggesting proper splicing. After sequencing, introns were absent from all cDNAs synthesized with primers spanning a single intron (**Fig. 2c**) or spanning both introns (except intron 1 + *lox*, suggesting altered splicing in this modified intron; **Supplementary Fig. 4b**). To assay ChR2 function, we transfected neuronal cultures (**Fig. 2d**) and obtained patch-clamp recordings (**Fig. 2e**). Photocurrents were comparable to those of native ChR2-EYFP except for those of intron 2 + *lox*, which were larger (ChR2-EYFP: 1,422 ± 92 pA, $n = 19$ neurons; intron 2 + *lox*: 2,279 ± 247 pA, $n = 5$ neurons, $P < 0.01$; mean ± s.e.m. given throughout). Neither exon fragment of ChR2 was able to generate photocurrents in isolation (**Supplementary Fig. 5**). Finally, to assay these constructs *in vivo*, we injected lentivirus into mouse medial prefrontal cortex (mPFC). All constructs were expressed by 1 week, and expression was sustained through at least 4 weeks (**Fig. 2f** and **Supplementary Fig. 6**). Together these results indicate that short introns inserted into the ChR2-EYFP coding sequence were properly spliced, did not impair gene function and enabled addition of heterologous sequence to the reading frame.

We next sought to optimize intron 1 given the impaired performance relative to that of intron 2. We identified differences between intron 1 and the consensus splice sequence[18,19]

(**Supplementary Fig. 4**), systematically changed these to match the consensus and then analyzed splicing by RT-PCR. The modified intron acceptor and intron 1 + *lox* template gave mixed products: one of these was the expected sequence, and the other was identical to the ChR2 sequence 139 bp 5′ to the expected splice site, likely revealing a cryptic splice site. Modification of either the exon or intron donor sequences produced a single, expected product, yet only the optimized intron donor sequence improved functional expression (ChR2-EYFP: 1,316 ± 120 pA, n = 8 neurons, intron donor: 2,219 ± 258 pA, n = 6 neurons,

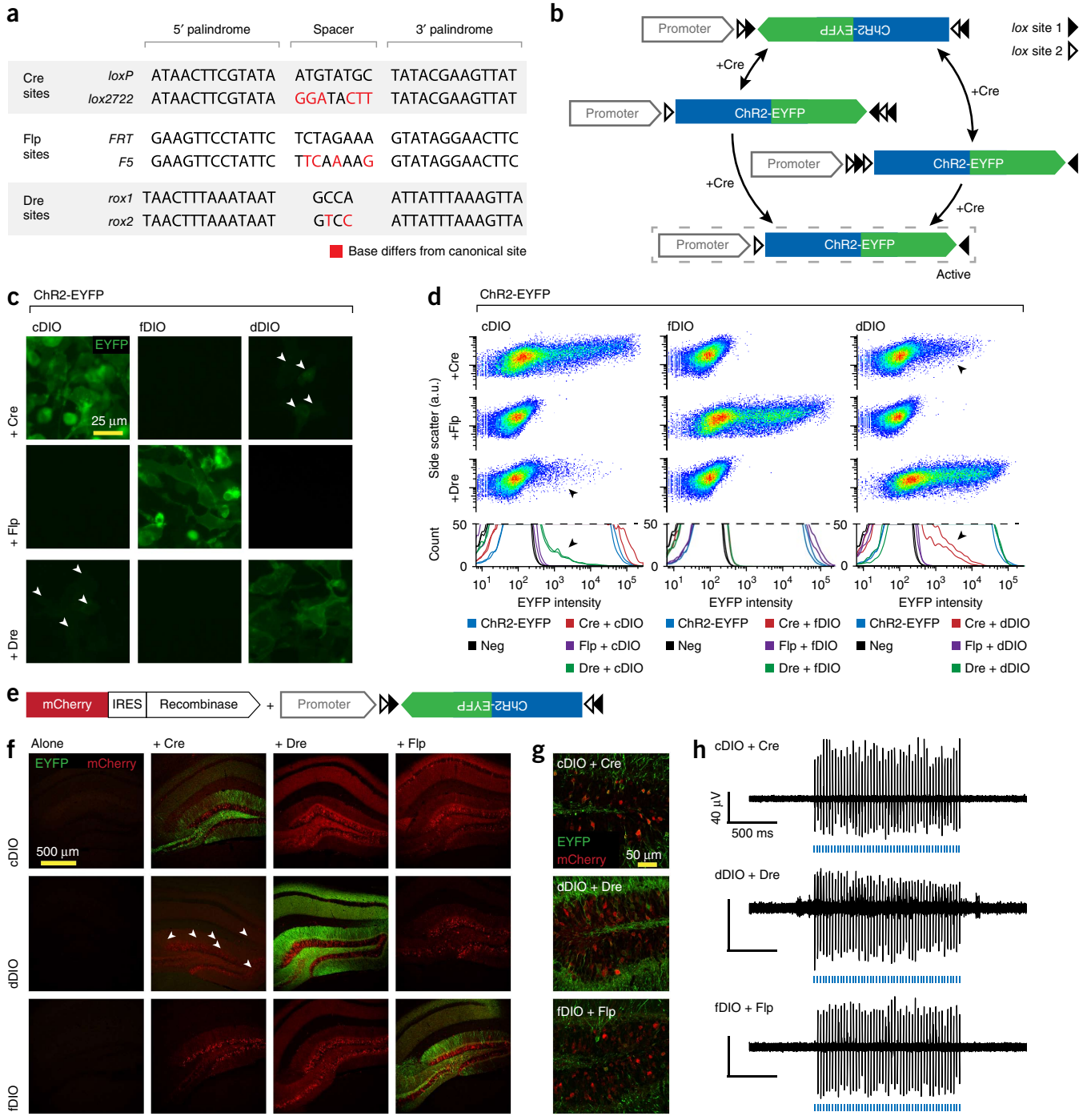

Figure 1 | Diversifying recombinase targeting strategies. (**a**) Recombinase recognition-site sequences used in DIO constructs. (**b**) Schematic of recombinase-mediated expression of a DIO construct. The ORF is initially inverted relative to the promoter and flanked by two sets of incompatible recombinase recognition sites. The recombinase first inverts the gene of interest into the forward orientation then either returns the gene to the starting position or excises two recognition sites and locks the gene in the forward orientation. (**c**) HEK293 cells transfected with recombinase-DIO combinations. Arrowheads indicate Cre and Dre cross-reactivity. (**d**) Flow cytometry analysis of cells from **c**. Dot plot (top) and histograms of biological replicates (n = 2; bottom) are shown. Arrowheads as in **c**. a.u., arbitrary units. (**e**) Schematic of viral vectors used in **f**–**h**. Each DIO was injected into mouse hippocampus alone or with a recombinase. (**f**,**g**) Recombinase-DIO expression *in vivo* at low (**f**) or high (**g**) magnification. Arrowheads indicate sparse expression with dDIO + Cre (**Supplementary Fig. 1**). (**h**) *In vivo* optrode recordings in animals co-injected with the indicated recombinase-DIO pairings.

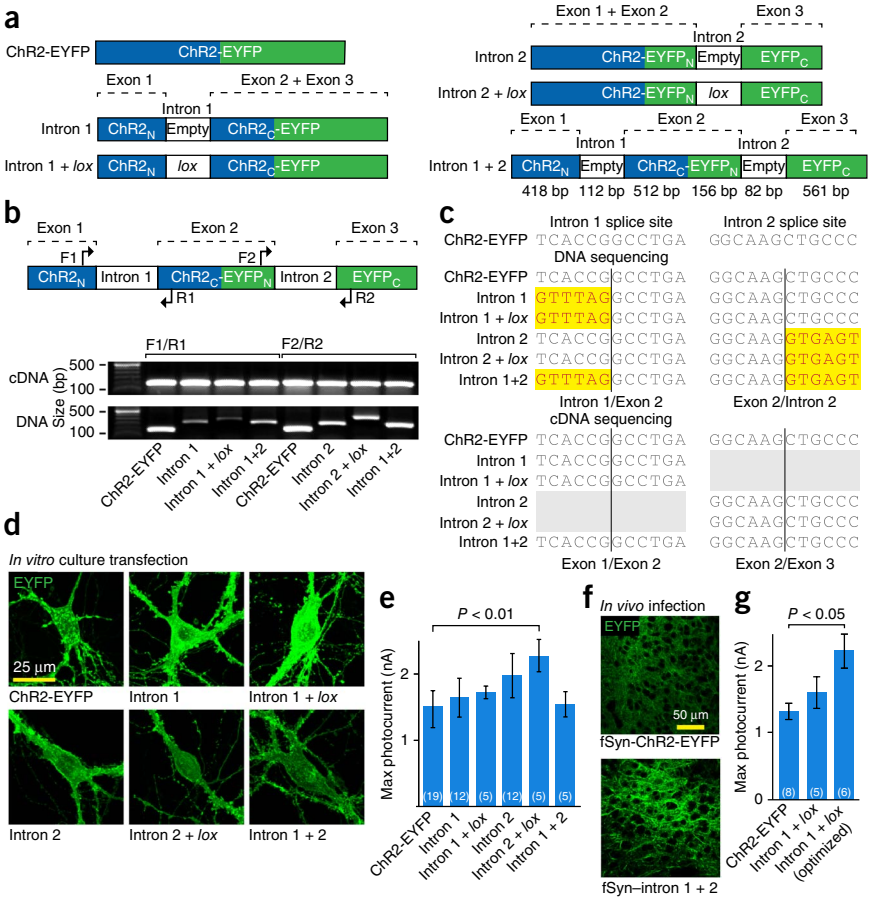

Figure 2 | Intron engineering for INTRSECT. (**a**) Schematic of constructs. 'Empty' denotes native introns; '*lox*' indicates addition of a *lox2722* site (Online Methods). (**b**) cDNA was prepared from mRNA of HEK293 cells transfected with the indicated constructs. Source DNA and cDNA were amplified by PCR with the indicated primers (top) and separated by gel electrophoresis (bottom). (**c**) Sequence of DNA isolated from bands in **b**. Yellow denotes differences from the ChR2-EYFP map sequence. (**d**) EYFP expression in primary neuronal cultures transfected with the indicated constructs. (**e**) Whole-cell photocurrents from primary neurons transfected with intron constructs (ChR2-EYFP, 1,422 ± 92 pA; intron 1, 1,591 ± 187 pA; intron 1 + *lox*, 1,722 ± 98 pA; intron 2, 1,862 ± 159 pA; intron 2 + *lox*, 2,279 ± 247 pA; intron 1 + intron 2, 1,540 ± 189 pA, $P < 0.01$, Dunnett's multiple comparison tests for ChR2-EYFP vs. intron 2 + *lox*). (**f**) Representative images, from at least 10 slices from 2 separately injected mPFC hemispheres, of EYFP expression in mPFC of mouse brain at 2 weeks post infection with lentivirus bearing the indicated constructs (**Supplementary Fig. 6**). (**g**) Whole-cell photocurrents illustrating increased peak photocurrent activity after intron 1 optimization (ChR2-EYFP, 1,316 ± 120 pA; intron 1 + *lox2722*, 1,603 ± 236 pA; intron donor, 2,219 ± 258 pA; $P < 0.05$, Dunnett's multiple comparison tests, ChR2-EYFP vs. intron donor; **Supplementary Fig. 4**). Error bars, s.e.m.; *n* values (number of cells) are indicated within bars.

$P < 0.05$; **Fig. 2g** and **Supplementary Fig. 4g**). We included this modification in all constructs using intron 1.

We next combined recombinases (Cre and Flp) and engineered introns, using the DIO strategy to independently manipulate ORF fragments. To target cells expressing Flp AND Cre (**Fig. 3a**), we inserted cDIO recombinase recognition cassettes in both introns and fDIO cassettes before and after the ChR2-EYFP coding sequence. Flp controlled the direction of the entire ORF, and the second exon was additionally controlled by Cre (**Fig. 3b**,**c**). Here we paired *loxN* (ref. 22) with *lox2722* and *F3* (ref. 17) with *F5* (**Supplementary Fig. 7**), eliminating *loxP* and *FRT* to prevent *trans* recombination[23] with legacy recognition sites in some transgenic animals. We configured the first and third exons in the antisense direction, reversing their order, and left the second in the sense direction (C_{on}/F_{on}-ChR2-EYFP; **Fig. 3b** and **Supplementary Fig. 8a**). Here, both recombinases are necessary to place all three exons into the sense configuration (**Fig. 3c**), and either recombinase alone cannot produce a complete reading frame for ChR2 or EYFP.

To assess splicing, we prepared cDNA from HEK293 cells cotransfected to express Cre, Flp and the C_{on}/F_{on}-ChR2-EYFP construct. A shift in band size between transfected DNA and cDNA was readily apparent (**Fig. 3d**); splicing was confirmed by sequencing (**Fig. 3e**). To assess functionality and specificity, we cotransfected cultured neurons or HEK293 cells with combinations of recombinases and C_{on}/F_{on}-ChR2-EYFP. EYFP expression was observed in only the neurons coexpressing Cre and Flp (**Fig. 3f** and **Supplementary Fig. 8a**), which is consistent with population flow cytometry data in HEK293 cells (100% of controls were fit by a single curve, and 100% of Cre-Flp cotransfections were fit by multiple curves; **Fig. 3g**). Neurons expressing Cre, Flp and either ChR2-EYFP or C_{on}/F_{on}-ChR2-EYFP had comparable photocurrents (**Fig. 3h**) and light-evoked action potentials (**Fig. 3i**). To examine functional specificity, we performed patch-clamp experiments while blinded to ChR2 expression, basing our selection of neurons to be patched solely on recombinase expression. We found photocurrents in only the triple-transfected condition (**Supplementary Fig. 9**). Last, we assessed the impact of expressing inactive configurations of C_{on}/F_{on}-ChR2-EYFP and observed no deleterious effects on membrane properties or cell survival (**Supplementary Fig. 10**). These data indicate that integrating multiple recombinases with heterologous introns is a viable strategy for intersectional expression dependent on Cre and Flp recombinases, with expression levels comparable to those of intron-free, non-recombinase-dependent counterparts.

Function of Cre and Flp–dependent ChR2-EYFP *in vivo*

We next tested our intersectional expression strategy *in vivo*. We bred double-transgenic PV-p2A-Cre;SOM-IRES-Flp mice—where PV is parvalbumin, IRES is an internal ribosome entry site and SOM is somatostatin—and injected wild-type, Cre, Flp or Cre;Flp mice with AAV-DJ-C_{on}/F_{on}-ChR2-EYFP driven by the human synapsin (hSyn) or EF1α/HTLV (nEF) promoters in dorsal CA1 of hippocampus and in mPFC. Rodent CA1 contains PV^+SOM^-, PV^-SOM^+ and PV^+SOM^+ neurons[24], whereas mPFC has PV^+SOM^- and PV^-SOM^+ neurons but lacks double-positive

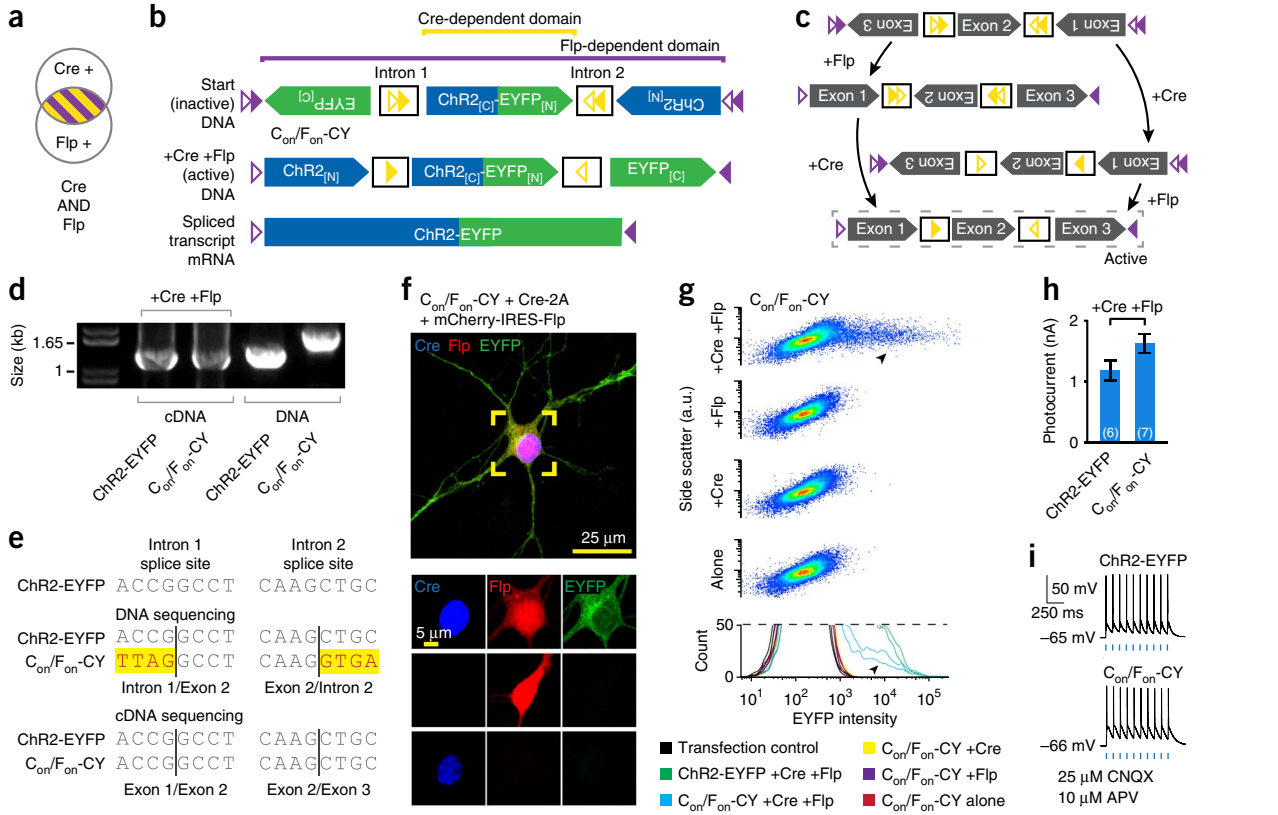

Figure 3 | INTRSECT: recombinases with engineered introns enable intersectional targeting *in vitro*. (**a**) Neurons expressing both Cre and Flp will express the transgene, but neurons expressing either recombinase alone will not. (**b**) Schematics showing a construct with expression dependent on both Cre and Flp. Cre-dependent directional control of the central exon and Flp-dependent directional control of all three exons result in both recombinases being necessary for all exons of the construct (C_{on}/F_{on}-ChR2-EYFP; C_{on}/F_{on}-CY for short) to be in the sense direction. (**c**) This strategy requires two DIO recombination events to occur in series; intermediate configurations in the activation of C_{on}/F_{on}-ChR2-EYFP are shown. Purple triangles, Flp recognition sites; yellow triangles, Cre recognition sites. (**d**) Construct DNA and cDNA prepared from HEK293 cells transfected with indicated constructs and recombinases were amplified using primers in exons 1 and 3 and separated by gel electrophoresis. (**e**) Sequences of bands from **d**. Yellow denotes differences from the ChR2-EYFP map sequence. (**f**) Cultured neuron transfected with C_{on}/F_{on}-ChR2-EYFP (green), Cre (blue) and Flp (red) (**Supplementary Fig. 8**). Lower panels show neurons expressing Cre or Flp alone. (**g**) Flow cytometry dot plot (top) and histograms of biological replicates ($n = 2$; bottom) of HEK293 cells transfected with indicated recombinase-construct combinations. a.u., arbitrary units. Arrowheads indicate histogram plot matched to exemplar dot plot. (**h**,**i**) Whole-cell photocurrents (**h**) and action potentials (**i**) recorded from primary neurons transfected with the indicated constructs (ChR2-EYFP, 1,120 ± 187 pA; C_{on}/F_{on}-ChR2-EYFP, 1,621 ± 157 pA; $P = 0.0625$, two-sided unpaired *t*-test). Error bars, s.e.m. *n* values (number of cells) are indicated. Synaptic transmission blockers CNQX and APV were used at the indicated concentrations.

PV$^+$SOM$^+$ cells[25]. With imaging maximized for sensitivity and with positive cells defined by fluorescence above background, hippocampal expression was restricted to double-transgenic Cre;Flp animals regardless of promoter (nEF: 6.5 cells per slice, $n = 37$ slices from 4 animals; hSyn: 8.2 cells per slice, $n = 52$ slices from 3 animals). Wild-type, PV-Cre and SOM-Flp animals displayed less than one cell per slice with fluorescence above background (**Fig. 4a**). No expression was observed in mPFC in any animal line (not shown).

We next analyzed ChR2 functionality in hippocampal slices prepared from PV-p2a-Cre;SOM-IRES-Flp animals injected with AAV-DJ-C_{on}/F_{on}-ChR2-EYFP driven by either hSyn or nEF. Using whole-cell patch clamp with biocytin-filled pipettes (**Fig. 4b**), we found robust photocurrents that reliably drove action potentials (**Fig. 4c**,**d**). To characterize the identity of recorded cells, we stained for PV, SOM and biocytin (**Fig. 4e**,**f**). Surprisingly, whereas all cells expressed SOM, only 8 of 27 were positive for PV, and even these were weakly stained. As some PV$^+$SOM$^+$ cells are known to express only minimal PV[26,27], we additionally processed slices for morphological characterization[28]. Of cells that were recovered with identifiable processes within the slice (17 of 33), 14 were classified as O-LM (oriens lacunosum moleculare), and the remaining 3 as bistratified (**Fig. 4e**,**f**); these cell types are known to express both PV and SOM[28].

To further characterize cells expressing C_{on}/F_{on}-ChR2-EYFP, we stained and imaged thin slices and obtained data consistent with slice patching results: most C_{on}/F_{on}-ChR2-EYFP–expressing cells examined were immunohistochemically PV^{low}SOM$^+$ or PV$^-$SOM$^+$ but were present only in PV$^+$SOM$^+$ animals (not in the single-marker transgenic lines; **Fig. 4g–j**). Recombinase transgene expression need not be restricted to cells readily identifiable by immunostaining[29]; we therefore crossed a separate PV-IRES-Cre mouse[30] with SOM-IRES-Flp. C_{on}/F_{on}-ChR2-EYFP expression was again limited to Cre;Flp double-transgenic mice (5.2 cells per slice, $n = 33$ slices), although with diminished fluorescence. Unlike in PV-p2a-Cre;SOM-IRES-Flp mice, expression was largely restricted to immunohistochemically PV$^+$SOM$^+$ cells (87% of cells PV$^+$SOM$^+$, $n = 173$ cells; **Fig. 4k**,**l**). Divergent

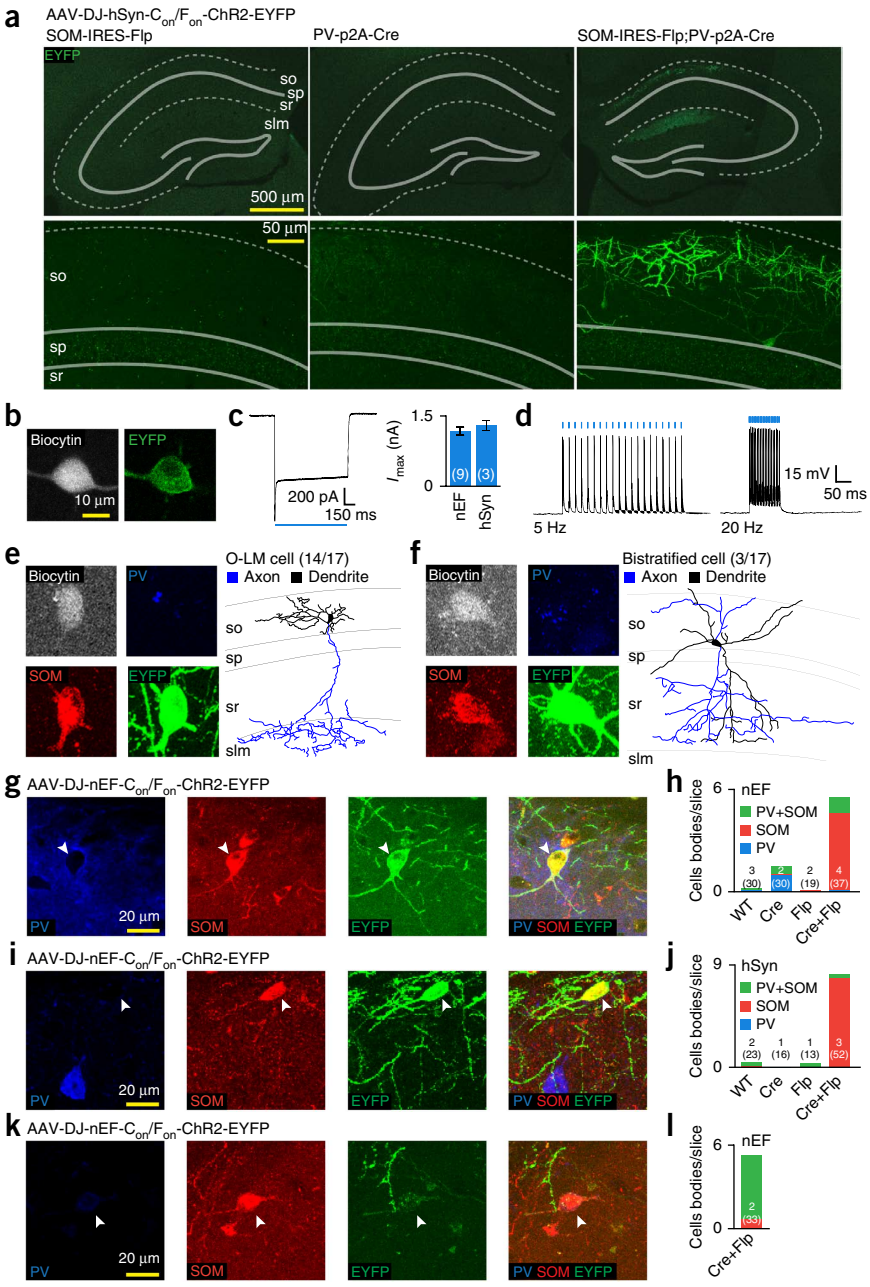

Figure 4 | INTRSECT specificity and functionality *in vivo*. (**a**) Hippocampal slices prepared 4 weeks after injection of the indicated animals with AAV-DJ-C_{on}/F_{on}-ChR2-EYFP. so, stratum oriens; sp, stratum pyramidale; sr, stratum radiatum; slm, stratum lacunosum moleculare. (**b**–**d**) $EYFP^+$ cells in PV-2a-Cre;SOM-IRES-Flp animals expressing C_{on}/F_{on}-ChR2-EYFP were patched with biocytin-filled pipettes (**b**) and assayed for peak photocurrent I_{max} (**c**) and action potentials (**d**). Error bars, s.e.m. (**e**,**f**) After patching, slices were stained for biocytin (gray), PV (blue) and SOM (red) for identification (left), which was followed by morphological reconstruction (right). All error bars s.e.m. All identified neurons were either oriens lacunosum moleculare (O-LM; 14 neurons) (**e**) or bistratified (**f**; 3 neurons) identified largely on a morphological basis. (**g**–**j**) Slices from PV-2a-Cre;SOM-IRES-Flp animals injected with virus driven by either hSyn or nEF, stained for SOM and PV (**g**,**i**), and cell numbers quantified in comparison to control animals (**h**,**j**). Arrowheads indicate $EYFP^+$ cells stained SOM^+ but PV^-. Injected animal number and (total hippocampal slices analyzed) are indicated on the bars. Imaging settings were optimized for sensitivity. (**k**,**l**) Micrographs (**k**) showing slices from PV-IRES-Cre;SOM-IRES-Flp mice injected in dorsal CA1 with the indicated construct. Cell numbers were quantified (**l**). Arrowheads indicate $EYFP^+$ cell stained SOM^+PV^+. WT, wild type.

expression of C_{on}/F_{on}-ChR2-EYFP in these double-transgenic mice is therefore likely driven by differences between the PV-p2a-Cre and PV-IRES-Cre transgenic lines themselves.

INTRSECT-based exclusion targeting: AND NOT

This modular intron-and-recombinase targeting strategy potentially facilitates additional expression logic through reorientation of exons within the standard backbone. We next sought to target cells expressing 'recombinase X AND NOT recombinase Y' (C_{on}/F_{off} and C_{off}/F_{on}; **Fig. 5a**) by manipulating exon starting direction (**Fig. 5a**,**b** and **Supplementary Fig. 8b**,**c**). We analyzed splicing in HEK293 cells and observed a large shift in cDNA amplicon size relative to transfected DNA (**Fig. 5c**) and confirmed successful splicing by sequencing (**Fig. 5d**). Neurons cotransfected with AND NOT constructs expressed ChR2-EYFP in the presence of the single activating recombinase but not in the presence of both Cre and Flp (**Fig. 5e**,**f** and **Supplementary Fig. 8b**,**c**), which was consistent with flow cytometry population data (multiple populations were fit in 85–96% of matched single-recombinase transfections, and a single population was fit in 94–99% of double-recombinase transfections; **Fig. 5g**). These constructs exhibited comparable peak photocurrents (**Fig. 5h**) and action potentials (**Fig. 5i**). We noted that C_{on}/F_{off}-ChR2-EYFP had a depressed photocurrent relative to that of non-recombinase-dependent ChR2-EYFP; unlike C_{on}/F_{on} or C_{off}/F_{on}, C_{on}/F_{off} contains a recombinase cassette upstream of the ORF when active, with two ATG sequences in the spacer; scrambling these sequences improved the photocurrent (**Supplementary Fig. 11**).

Other applications, such as expression of fluorescent proteins alone, require adaptation of these multiple-recombinase tools to a single ORF. We achieved this by modifying the intron approach for use with EYFP (**Supplementary Fig. 12**). Here, the 5′ and 3′ halves of EYFP are under control of separate recombinases, with a single intron containing Cre and Flp DIO cassettes. RT-PCR analysis using direction-specific primers suggested that EYFP sequence in C_{on}/F_{on}, C_{on}/F_{off} and C_{off}/F_{on} variants was amplified from recombinase-cotransfected HEK293 cells, but not source DNA, and was verified by sequencing. Flow cytometry

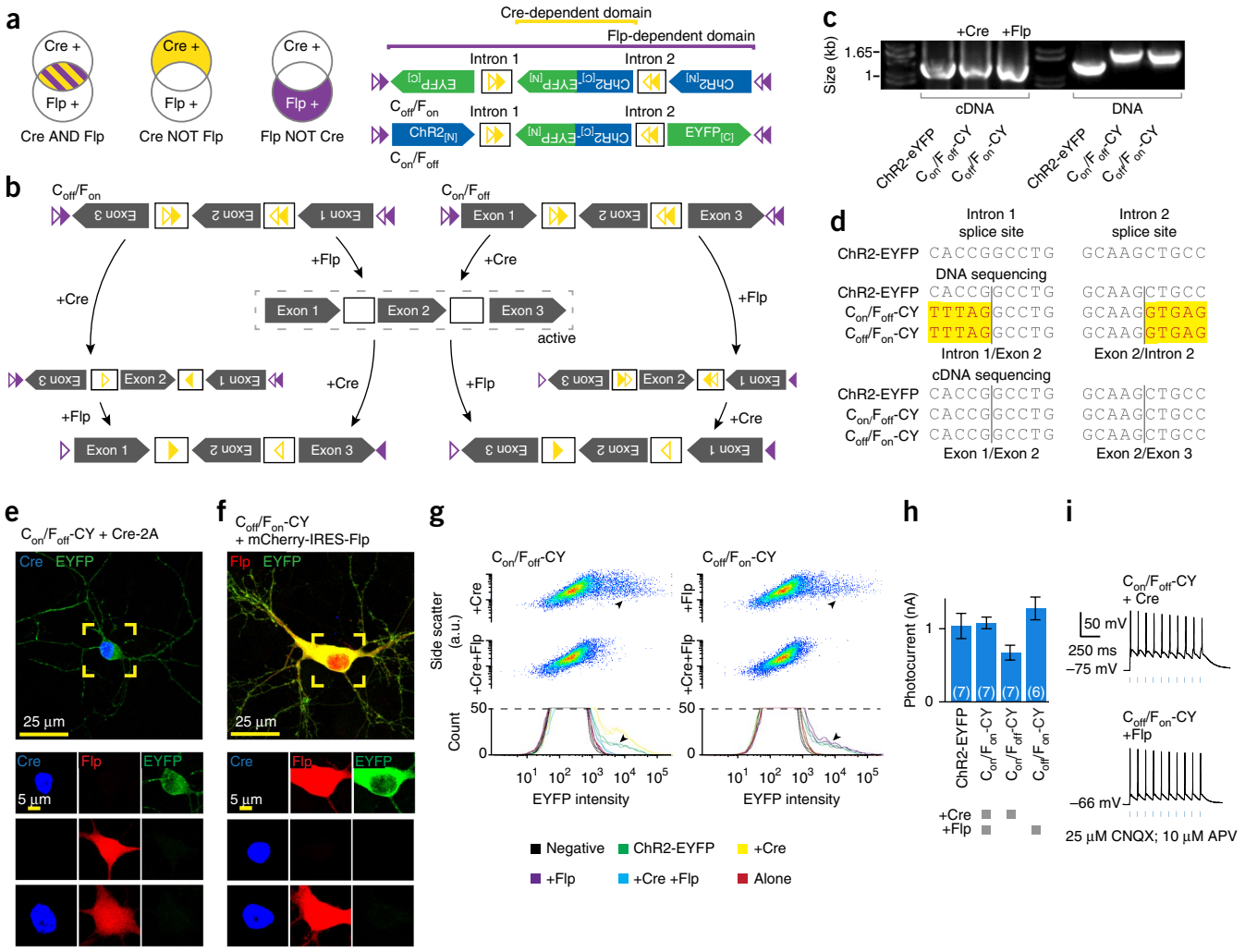

Figure 5 | Exclusion logic using INTRSECT. (**a**) Schematics representing target populations of cells expressing Cre and Flp (left) by nesting Cre-dependent directional control of a central exon and Flp-dependent directional control of all three exons (right). (**b**) Intermediate states driven by Cre and Flp on constructs dependent on the exclusive presence of a single recombinase for functional expression (dashed box). (**c**) cDNA and construct DNA prepared from HEK293 cells transfected with indicated constructs and recombinases were amplified by PCR with primers in exons 1 and 3 and separated by gel electrophoresis. (**d**) Sequences of bands from **b**. Yellow denotes differences from the ChR2-EYFP map sequence. (**e**,**f**) Cultured neurons transfected with combinations of Cre (blue), Flp (red), and C_{on}/F_{off} (**e**; green) or C_{off}/F_{on} (**f**; green). Lower images show neurons expressing inactive combinations of Cre and Flp. (**g**) Flow cytometry dot plot (top) and histograms of biological replicates (n = 2; bottom) of HEK293 cells transfected with indicated recombinase-construct combinations. Arrowheads indicate expression in the presence of a single recombinase. a.u., arbitrary units. (**h**,**i**) Whole-cell photocurrents (**h**) and action potentials (**i**) recorded from primary neurons transfected with the indicated constructs. Error bars, s.e.m.; n values (number of cells) are indicated.

indicated that EYFP was expressed only after cotransfection with appropriate recombinases, including AND NOT configurations, 5 days after transfection.

Projection targeting using multiple recombinases

We next combined fDIO and cDIO with projection-targeting strategies in order to restrict expression to cells defined by both genetic identity and projection pattern. Targeting dopaminergic (DA) cells of the ventral tegmental area (VTA) projecting to the nucleus accumbens (NAc) requires an intersectional strategy as neither all VTA-DA neurons (which project to numerous downstream areas) nor the entire VTA-NAc projection (which includes DA and non-DA cells[31]) describes this population. We confirmed that projection-based targeting alone was insufficient by injecting the retrograde virus LT-HSV-mCherry-IRES-Cre (**Fig. 6a** and **Supplementary Fig. 13**) into NAc and AAV-cDIO-ChR2-EYFP into VTA of wild-type mice (**Fig. 6b**): only 48% of VTA EYFP$^+$ cells were positive for tyrosine hydroxylase (TH; the rate-limiting enzyme in dopamine production; **Fig. 6c**,**d**). To target DA VTA-NAc neurons, we injected LT-HSV-lox-STOP-lox-mCherry-IRES-Flp into NAc of TH-Cre transgenic mice and AAV5-fDIO-ChR2-EYFP into VTA (**Fig. 6e**). Only VTA neurons that both express Cre (TH$^+$) and are transduced by LT-HSV (NAc projecting) should express Flp and therefore activate fDIO-ChR2-EYFP. Indeed, 94% of VTA EYFP$^+$ cells were clearly mCherry$^+$, and 93% of VTA EYFP$^+$ cells were TH$^+$; 60% of mCherry$^+$TH$^+$ cells were EYFP$^+$ (**Fig. 6f**,**g**). EYFP$^+$ fibers were abundant in NAc (**Fig. 6f**) but absent in the mPFC and basolateral amygdala, as expected[32]. Occasional sparse EYFP$^+$ fibers but no cell bodies were seen in negative controls lacking either Cre or Flp (**Supplementary Fig. 14**).

Extension of INTRSECT

The modular design of INTRSECT opens the door to additional logical operations, including XOR, NAND and others (**Supplementary Fig. 15**). As criteria differentiating cell types become more sophisticated, three-term Boolean logic may become desirable (for example, a AND b AND c), heightening the value of identifying new recombinases, such as Cre relatives VCre and SCre[33]. In preliminary work, we synthesized human codon–optimized VCre and SCre, created vcDIO- and scDIO-ChR2-EYFP vectors, and transfected these alongside Cre, Flp and Dre in HEK293 cells (**Fig. 6h**). Although scDIO/SCre did not function well, VCre induced EYFP expression in vcDIO-ChR2-EYFP (100% of samples fit to multiple curves) without cross-activity (93–98% of off-target DIOs were fit with a single curve; **Fig. 6h**).

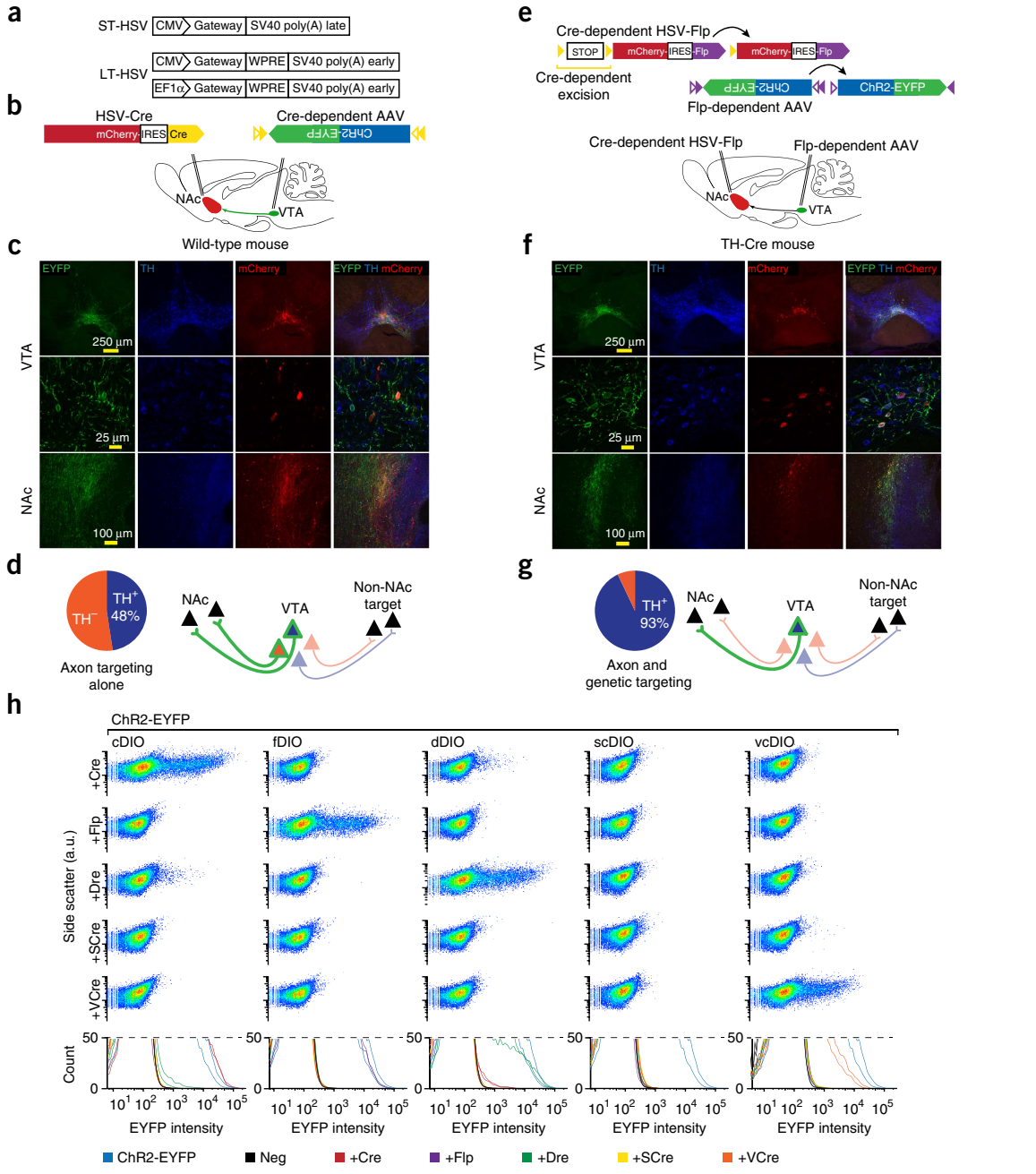

Figure 6 | Combinatorial targeting with multiplexed recombinases. (**a**) Schematics comparing short-term (ST-HSV) and optimized long-term (LT-HSV) vectors. EF1α promoter used for all experiments unless otherwise indicated. (**b**) The approach for projection-based targeting of the nucleus accumbens (NAc)-projecting ventral tegmental area (VTA) cells in a wild-type mouse is shown. Note that LT-HSV-mCherry-IRES-Cre is a retrograde vector. (**c**,**d**) *In vivo* expression pattern of the indicated markers (**c**) and model of the data (**d**) for the projection-based targeting schematized in **b**. Robust EYFP expression was observed within VTA, colocalized with TH in only 48% (69/145) of cells. (**e**) Strategy for combination projection-genetic targeting of the NAc-projecting TH$^+$ VTA cells in a TH-IRES-Cre mouse. (**f**,**g**) *In vivo* expression pattern of the indicated markers (**f**) and model of the data (**g**) for combination projection–genetic-based targeting schematized in **e**. EYFP expression in the VTA was highly colocalized with TH staining (145/156 cells). (**h**) Flow cytometry dot plot (top) and histograms of biological replicates (n = 2; bottom) of HEK293 cells transfected with indicated recombinase-construct combinations. Neg, negative control; a.u., arbitrary units.

DISCUSSION

In defining the function of specific cell types, precise targeting has been a long-standing limitation, with expression of genetically encoded tools generally constrained to populations defined by a single feature. To meet challenges of multifeature targeting, we have developed and validated a flexible, modular and generalized approach integrating multiple recombinases, intron engineering and specialized viruses (INTRSECT).

Contrary to previous reports of Cre-Dre independence[16] we observed Cre/*rox* cross-reaction *in vitro* and *in vivo*. Cre and Dre are both phage derived, with recognition sites sharing high homology in the 13-bp palindromic region that determines recombinase pairing. Sites used here could contribute to this cross-reaction, and other noncanonical sites may allow for their combined use. In any case, our results with Flp buttress its independence from Cre and establish it for the first time with Dre.

The multiple-recombinase and viral methods used in INTRSECT may synergize with strategies for tracing connectivity across networks, such as engineered viruses[34]. It will be important to validate penetrance, specificity and safety of viral tools in each system. In this regard, although we observed minimal inappropriate expression with our constructs, AAVs can form end-to-end concatemers with payload deletion and rearrangement[35], a process that may induce expression in isolation[36] and could contribute (along with low TH expression) to the small population of TH$^-$ cells in projection-targeting experiments (**Fig. 6f**,**g**). Alternatively, read-through in HSV lox-STOP-lox cassettes is possible, separate from INTRSECT constructs[7,10], and may be improved by alternative strategies (**Supplementary Fig. 16a**). However, the absence of inappropriate expression in controls (**Supplementary Fig. 14**) suggests instead that targeting NAc-projecting cells may enrich for rare VTA TH$^-$ cells labeled by this transgenic line[8,32].

To create a single-AAV–based system capable of performing diverse Boolean logic on expression patterns, we built upon a substantial intron literature. Pioneering work adding heterologous introns to mammalian transgenes revealed that introns may function as independent units and that their addition to cDNAs can improve expression *in vitro*[20,37] and *in vivo*[38], which is consistent with our findings that introns inserted into ChR2-EYFP are spliced and enhance photocurrents. The use of intron-containing fluorophores may facilitate integrating introns into genetic tools for increased expression. We relied on splice-site descriptions[18,19] in optimizing INTRSECT constructs and found that improved splicing correlated with increased photocurrents, emphasizing potential benefits of heterologous introns. For future work requiring additional introns, many options exist, although it may be sufficient to duplicate the two used here[39].

The targetability of these cells will now allow for experiments characterizing their role in behavior, and together with C_{on}/F_{off} and C_{off}/F_{on}, these reagents may be of immediate utility in studies of interneuron modulation of hippocampal function[27]. For future work, validation of targeting in each system with multiple approaches is indicated. Here we used immunohistochemistry and morphologic analysis of targeted hippocampal cells; electrophysiological and other properties may also be employed. Differences observed in targeted cell types between similar transgenic mouse lines underscore the importance of considering recombinase expression pattern in transgenic animals, including bicistronic knock-ins. Production of additional transgenic animals expressing Flp will augment options for targeting refined cell populations.

Individual components of the INTRSECT system, including viral, recombinase and intron tools, may be separated or combined, as we have shown in targeting the NAc-projecting DA cells of the VTA. Beyond this example, cells in an 'upstream' brain region that project to two different downstream regions could be targeted to either include or exclude neurons according to projection pattern and may be combined with transgenic recombinase mouse lines for additional specificity (**Supplementary Fig. 16**). And although we have used ChR2-EYFP as a single targeted gene here, these tools also enable independent targeting and manipulation of multiple separately defined cell types within a single animal (**Supplementary Fig. 16d**). INTRSECT tools have a modular design, may be integrated with existing reagents and animals, and may enable diverse expression logic for genetically encoded tools based on multiple genetic and/or connectivity factors.

METHODS

Methods and any associated references are available in the online version of the paper.

Note: Any Supplementary Information and Source Data files are available in the online version of the paper.

ACKNOWLEDGMENTS

We thank M. Kay (Stanford) for providing the pRC-DJ plasmid used to produce AAV-DJ; M. Bigos at the Stanford Shared FACS Facility for assistance with experiment planning and data analysis; S. Roy for extensive discussions regarding intron function and structure; P. Wu for technical assistance in mouse engineering and characterization; and the entire Deisseroth lab for helpful discussions. The Neuroscience Gene Vector and Virus Core at Stanford is funded in part by US National Institutes of Health grant # NINDS P30 NS069375-01A1. This work is supported by the Stanford Medical Scientist Training Program (MSTP; L.E.F. and J.M.), a Stanford Bio-X Fellowship (J.M. and M. Hyun), the Samsung Scholarship (M. Hyun), the Robertson Neuroscience Fund of Cold Spring Harbor Laboratory (M. He, J.T. and Z.J.H.), the Stony Brook University MSTP (J.T.), a Howard Hughes Medical Institute International Student Fellowship (A.S.), National Science Foundation (NSF) grant 0801700 (L.G.), the NSF Graduate Research Fellowship Program (K.A.Z.), the New York University MSTP (H.B.), the Human Frontiers Science Project and German Academic Exchange Service (DAAD; I.D.), and US National Institute on Drug Abuse (NIDA) DA024763 (C.E.B.). K.D. is supported by the Wiegers Family Fund, US National Institute of Mental Health, NIDA, Defense Advanced Research Projects Agency REPAIR Program, Keck Foundation, McKnight Foundation, Gatsby Charitable Foundation, Snyder Foundation, Woo Foundation, Tarlton Foundation, and Albert Yu and Mary Bechman Foundation. All tools and methods are distributed and supported freely at http://www.optogenetics.org/ and Addgene.

AUTHOR CONTRIBUTIONS

L.E.F., J.M., C.R. and K.D. designed the study and interpreted results. L.E.F., J.M. and K.D. wrote the paper. L.E.F. and J.M. coordinated the experiments. L.E.F., J.M., S.Y.L., A.B. and A.S. performed *in vitro* electrophysiology experiments. J.M. and K.A.Z. performed *in vivo* electrophysiology experiments. L.E.F., J.M., M. Hyun, A.S., K.A.Z., H.B. and I.D. performed viral injections. L.E.F., J.M., M. Hyun, S.Y.L., J.T., K.A.Z., H.B., H.S., I.D. and C.P. performed immunohistochemistry. L.E.F., C.R., R.N., C.E.B. and F.M.B. provided viruses. L.G., J.M. and L.E.F. performed statistical analysis. L.E.F., J.M., C.R., M. Hyun, A.B. and C.P. performed molecular engineering and characterization. M. He, J.T. and Z.J.H. provided animals. All authors contributed to editing. K.D. supervised all aspects of the project.

COMPETING FINANCIAL INTERESTS

The authors declare no competing financial interests.

1. Crick, F.H. Thinking about the brain. *Sci. Am.* **241**, 219–232 (1979).
2. Boyden, E.S., Zhang, F., Bamberg, E., Nagel, G. & Deisseroth, K. Millisecond-timescale, genetically targeted optical control of neural activity. *Nat. Neurosci.* **8**, 1263–1268 (2005).
3. Yizhar, O., Fenno, L.E., Davidson, T.J., Mogri, M. & Deisseroth, K. Optogenetics in neural systems. *Neuron* **71**, 9–34 (2011).
4. Luo, L., Callaway, E.M. & Svoboda, K. Genetic dissection of neural circuits. *Neuron* **57**, 634–660 (2008).
5. Zhang, F. in *Neuronal Circuits: From Structure to Function* (Cold Spring Harbor Laboratory, 2008).
6. Atasoy, D., Aponte, Y., Su, H.H. & Sternson, S.M. A FLEX switch targets Channelrhodopsin-2 to multiple cell types for imaging and long-range circuit mapping. *J. Neurosci.* **28**, 7025–7030 (2008).
7. Sohal, V.S., Zhang, F., Yizhar, O. & Deisseroth, K. Parvalbumin neurons and gamma rhythms enhance cortical circuit performance. *Nature* **459**, 698–702 (2009).
8. Tsai, H.C. *et al.* Phasic firing in dopaminergic neurons is sufficient for behavioral conditioning. *Science* **324**, 1080–1084 (2009).
9. Saunders, A., Johnson, C.A. & Sabatini, B.L. Novel recombinant adeno-associated viruses for Cre activated and inactivated transgene expression in neurons. *Front. Neural Circuits* **6**, 47 (2012).
10. Kuhlman, S.J. & Huang, Z.J. High-resolution labeling and functional manipulation of specific neuron types in mouse brain by Cre-activated viral gene expression. *PloS ONE* **3**, e2005 (2008).
11. Awatramani, R., Soriano, P., Rodriguez, C., Mai, J.J. & Dymecki, S.M. Cryptic boundaries in roof plate and choroid plexus identified by intersectional gene activation. *Nat. Genet.* **35**, 70–75 (2003).
12. Siuti, P., Yazbek, J. & Lu, T.K. Synthetic circuits integrating logic and memory in living cells. *Nat. Biotechnol.* **31**, 448–452 (2013).
13. Marti, T. Refolding of bacteriorhodopsin from expressed polypeptide fragments. *J. Biol. Chem.* **273**, 9312–9322 (1998).
14. Schmitt, C. *et al.* Specific expression of Channelrhodopsin-2 in single neurons of *Caenorhabditis elegans*. *PLoS ONE* **7**, e43164 (2012).
15. Raymond, C.S. & Soriano, P. High-efficiency FLP and PhiC31 site-specific recombination in mammalian cells. *PLoS ONE* **2**, e162 (2007).
16. Sauer, B. & McDermott, J. DNA recombination with a heterospecific Cre homolog identified from comparison of the pac-c1 regions of P1-related phages. *Nucleic Acids Res.* **32**, 6086–6095 (2004).
17. Schlake, T. & Bode, J. Use of mutated FLP recognition target (FRT) sites for the exchange of expression cassettes at defined chromosomal loci. *Biochemistry* **33**, 12746–12751 (1994).
18. Mount, S.M. A catalogue of splice junction sequences. *Nucleic Acids Res.* **10**, 459–472 (1982).
19. Zhang, M.Q. Statistical features of human exons and their flanking regions. *Hum. Mol. Genet.* **7**, 919–932 (1998).
20. Chapman, B.S., Thayer, R.M., Vincent, K.A. & Haigwood, N.L. Effect of intron A from human cytomegalovirus (Towne) immediate-early gene on heterologous expression in mammalian cells. *Nucleic Acids Res.* **19**, 3979–3986 (1991).
21. Ishida, N., Ueda, S., Hayashida, H., Miyata, T. & Honjo, T. The nucleotide sequence of the mouse immunoglobulin epsilon gene: comparison with the human epsilon gene sequence. *EMBO J.* **1**, 1117–1123 (1982).
22. Livet, J. *et al.* Transgenic strategies for combinatorial expression of fluorescent proteins in the nervous system. *Nature* **450**, 56–62 (2007).
23. Zong, H., Espinosa, J.S., Su, H.H., Muzumdar, M.D. & Luo, L. Mosaic analysis with double markers in mice. *Cell* **121**, 479–492 (2005).
24. Somogyi, P. & Klausberger, T. Defined types of cortical interneurone structure space and spike timing in the hippocampus. *J. Physiol.* (*Lond.*) **562**, 9–26 (2005).
25. Kawaguchi, Y. & Kubota, Y. GABAergic cell subtypes and their synaptic connections in rat frontal cortex. *Cereb. Cortex* **7**, 476–486 (1997).
26. Ferraguti, F. *et al.* Immunolocalization of metabotropic glutamate receptor 1α (mGluR1α) in distinct classes of interneuron in the CA1 region of the rat hippocampus. *Hippocampus* **14**, 193–215 (2004).
27. Klausberger, T. *et al.* Brain-state- and cell-type-specific firing of hippocampal interneurons *in vivo*. *Nature* **421**, 844–848 (2003).
28. Klausberger, T. GABAergic interneurons targeting dendrites of pyramidal cells in the CA1 area of the hippocampus. *Eur. J. Neurosci.* **30**, 947–957 (2009).
29. Madisen, L. *et al.* A robust and high-throughput Cre reporting and characterization system for the whole mouse brain. *Nat. Neurosci.* **13**, 133–140 (2010).
30. Hippenmeyer, S. *et al.* A developmental switch in the response of DRG neurons to ETS transcription factor signaling. *PLoS Biol.* **3**, e159 (2005).
31. Van Bockstaele, E.J. & Pickel, V.M. GABA-containing neurons in the ventral tegmental area project to the nucleus accumbens in rat brain. *Brain Res.* **682**, 215–221 (1995).
32. Stamatakis, A.M. *et al.* A unique population of ventral tegmental area neurons inhibits the lateral habenula to promote reward. *Neuron* **80**, 1039–1053 (2013).
33. Suzuki, E. & Nakayama, M. VCre/VloxP and SCre/SloxP: new site-specific recombination systems for genome engineering. *Nucleic Acids Res.* **39**, e49 (2011).
34. Wickersham, I.R. *et al.* Monosynaptic restriction of transsynaptic tracing from single, genetically targeted neurons. *Neuron* **53**, 639–647 (2007).
35. Yang, J. *et al.* Concatamerization of adeno-associated virus circular genomes occurs through intermolecular recombination. *J. Virol.* **73**, 9468–9477 (1999).
36. Nakai, H., Storm, T.A. & Kay, M.A. Increasing the size of rAAV-mediated expression cassettes *in vivo* by intermolecular joining of two complementary vectors. *Nat. Biotechnol.* **18**, 527–532 (2000).
37. Buchman, A.R. & Berg, P. Comparison of intron-dependent and intron-independent gene expression. *Mol. Cell. Biol.* **8**, 4395–4405 (1988).
38. Palmiter, R.D., Sandgren, E.P., Avarbock, M.R., Allen, D.D. & Brinster, R.L. Heterologous introns can enhance expression of transgenes in mice. *Proc. Natl. Acad. Sci. USA* **88**, 478–482 (1991).
39. Reed, R. & Maniatis, T. A role for exon sequences and splice-site proximity in splice-site selection. *Cell* **46**, 681–690 (1986).

ONLINE METHODS

Statistical analysis. All statistical tests were chosen on the basis of normality of data and appropriateness of comparison to be analyzed by a particular approach. Data that were not normally distributed were either transformed to achieve normality or analyzed with a test that does not assume normal distribution. Estimation of variance was performed by Bartlett's test for equal variance (for ANOVAs) or by an *F*-test to compare variance (for unpaired *t*-tests). Variances were equal except when explicitly noted below. All error bars are reported as s.e.m.

Figure 2e. $n = 19$ for ChR2-EYFP group, $n = 12$ for intron 1 group, $n = 5$ for intron 1 + *lox* group, $n = 12$ for intron 2 group, $n = 5$ for intron 2 + *lox* group, $n = 5$ for intron 1 + 2 group. One-way type I ANOVA detected significant difference between the means: $F_{5,52} = 2.856$, $P = 0.0237$. ChR2 and intron 2 + *lox* showed significant differences: $P < 0.01$, Dunnett's multiple comparison test. Results were pooled from data acquired across multiple transfections after ensuring that there were no significant within-construct differences across those transfections.

Figure 2g. $n = 8$ for fSyn-ChR2-EYFP group, $n = 5$ for intron 1 + *lox* group, $n = 6$ for iC4A group ("intron 1 + *lox* optimized"). fSyn-ChR2-EYFP and iC4A showed significant differences: $P < 0.05$, Dunnett's multiple comparison test.

Figure 3h. $n = 6$ for ChR2 group, $n = 7$ for C_{on}/F_{on} group. Unpaired two-sided *t*-test showed no significant difference: $P = 0.0625$.

Figure 5h. $n = 7$ for fSyn-ChR2-EYFP group, $n = 7$ for C_{on}/F_{on} group, $n = 7$ for C_{on}/F_{off} group, $n = 6$ for F_{on}/C_{off} group. One-way type I ANOVA detected significant difference between the means: $F_{3,23} = 3.553$, $P = 0.0301$. No significant differences were detected by Dunnett's multiple comparison tests.

Molecular cloning. All single recombinase–dependent plasmids were constructed in an AAV-Ef1α backbone using the double-floxed inverted open-reading-frame (DIO) strategy described previously[7,8]. For construction of Flp-dependent recombinant AAV vectors, a DNA cassette carrying two pairs of incompatible *FRT* sites (*FRT* and *F5* (ref. 17)) was synthesized, and the ChR2-EYFP transgene was inserted between the two sites in the reverse orientation. The resulting cassette was cloned into a modified version of the pAAV2-MCS vector carrying the Ef1α promoter and the woodchuck hepatitis virus post-transcriptional regulatory element (WPRE) to enhance expression. A similar strategy was used to construct the Dre-dependent plasmids, except because there was only one known *rox* site[16], a novel *rox* site (*rox2*) was designed (5′-aactttaaataatgtcgattatttaaagtta-3′).

Three constructs were used to deliver *cre* into cells either *in vivo* or *in vitro*: AAV-Ef1α-Cre, AAV-Ef1α-Cre-p2A, AAV-EF1α-mCherry-IRES-Cre. The p2A peptide sequence was added where indicated as an immunostaining antigen. Similar constructs were used for Flp, Dre, VCre and SCre. Dre, VCre and SCre were human codon optimized and synthesized (DNA2.0). All AAV vectors were tested for *in vitro* expression before viral production. Updated maps are available at http://optogenetics.org/.

To create early multiple recombinase–dependent constructs, we used two separate approaches to modifying cDIO-hChR2(H134R)-EYFP. The first was by inverting the Ef1α promoter and flanking it with (5′ of the promoter) *FRT* and *F5* in the forward direction and (3′ of the promoter) *F5* and *FRT* in the reverse direction. This construct effectively has two tandem DIO cassettes: one that encompasses the promoter and one that encompasses the ORF; thus, it was named 'double-inverted promoter/double-inverted ORF (DIP/DIO)' AAV-fDIP EF1a-cDIO hChR2 (H134R)-EYFP. Second, three other Cre- and Flp-dependent variants were created by leaving the promoter in the forward direction but nesting Flp recognition sites such that the 5′ forward direction sites were within one of the extracellular loops of ChR2 and the 3′ reverse direction sites were situated beyond the STOP codon. The portion of the ChR2 reading frame within the Flp recognition sites is initially in the forward direction, and the portion of the reading frame under control of only Cre is initially in the reverse direction. This second strategy retains an *F5* site within the coding frame of ChR2 in the active conformation that occurs after the recombination catalyzed by Cre and Flp.

Short introns identified by a literature search (Intron 1: CMV Towne Variant intron B (ref. 20), GenBank M60321; Mouse IgE intron 3 (ref. 21), GenBank X01857.1) and derivatives were synthesized as oligonucleotides (oligos) and inserted by overlapping PCR directly into the ORF of ChR2 or EYFP as indicated. Target sites for insertion were determined using two criteria: first, that the two bases 5′ and the two bases 3′ of the insertion site match the exonic 5′ and 3′ consensus splice-site sequences, respectively; and second, that it would be unlikely that either fragment upstream or downstream of the reading frame translated in isolation would encode a functional protein. Splicing was tested *in silico* using NetGene2 (ref. 40; http://www.cbs.dtu.dk/services/NetGene2/). To test intron function, these modified ChR2-EYFP fusion genes were inserted into a lentiviral backbone driven by the human synapsin (hSyn) promoter between BamHI and EcoRI, scaled up and purified using endotoxin-free (Qiagen endotoxin-free MaxiPrep) or low endotoxin (Invitrogen MaxiCard) plasmid preparation kits for small-batch lentiviral production.

To introduce recombinase recognition sites and enable directional control of individual exons, we first constructed a standard AAV backbone with a multiple cloning site downstream of either the hSyn or chimeric EF1α/HTLV promoter consisting (from 5′ to 3′) of BamHI, AscI, SalI, SpeI, KpnI, NheI, XbaI and EcoRI through oligo ligation. We next identified likely donor, branch-point and acceptor regions in the intron by comparison to consensus sequences[18,19]. Proper exon-exon joining was ensured by directly joining the donor and acceptor sequences for each intron to their exonic partners, using overlapping PCR, without intervening restriction sites. To incorporate Flp control of all three exons, we separated incompatible sites[17] *F3* and *F5* by a short spacer sequence[8] and placed them between BamHI and AscI in the sense direction and between XbaI and EcoRI in the antisense direction. To incorporate Cre control of the second exon, we separated incompatible sites[22] *lox2722* and *loxN* by the same spacer sequence and fused them in the sense direction to the CMV (intron 1) bp and intronic sequence and in the antisense direction to the IgE (intron 2) bp and intronic sequence and placed them between the SalI and SpeI and KpnI and NheI sites, respectively. *F3* and *loxN* were chosen over *FRT* and *loxP* to decrease the possibility of chromosomal translocation[23] in transgenic animals that harbor either of these sites in their genome as legacy sequence from antibiotic resistance cassettes used during animal production. With this standard acceptor vector, exon direction for each Boolean value was determined, correct

restriction sites were placed on exons via PCR addition and exons were ligated into the AAV acceptor vector. DNA was amplified as above for production of AAV. All constructs are freely available (http://www.optogenetics.org/).

Construct variants for control experiments were built as follows: truncated ChR2 for exon function experiments were created by (i) fusing the 3′ end of the exon 1 in-frame to EYFP, adding bases as necessary and (ii) fusing the 3′ end of the ChR2 portion of exon 2 to EYFP, adding an ATG start codon to the 5′ end and bases as necessary to the 3′ end to create a functional reading frame. Constitutive blue fluorescent protein (BFP) was added to constructs for cell health experiments by creating a BFP expression cassette consisting (5′ to 3′) of the hSyn promoter, BFP and poly(A) tail. This was then cloned into a unique MluI site 5′ of the hSyn promoter driving expression of cDIO-ChR2-EYFP, fDIO-ChR2-EYFP or C_{on}/F_{on}-ChR2-EYFP such that it was independently expressed from the recombinase-dependent expression cassette.

Flow cytometry. HEK293FT cells (Invitrogen) were grown in 24-well tissue culture plates to 90% confluence and transfected in duplicate with 800 ng total DNA with Lipofectamine 2000 (Invitrogen) following the manufacturer protocol. HEK cells were not routinely screened for *Mycoplasma*. Five days post transfection, cells were removed by enzymatic dissociation (TrypLE, Gibco), resuspended in PBS, pelleted at 200*g* for 5 min and resuspended in 500 µL PBS supplemented with 1 µg/mL propidium iodide (PI; Sigma), and then placed on ice under aluminum foil until analysis. Flow cytometry was completed on a Scanford analyzer at the Stanford Shared FACS Facility using settings optimized for side scatter (SS), forward scatter (FS), PI and EYFP acquisition using positive (ChR2-EYFP), negative (empty transfection) and dead (heat-killed; 95 °C for 3 min) conditions as controls. Live-cell populations used in comparisons were isolated from debris and dead cells in *post hoc* analysis by (i) negatively gating for PI^+ cells and (ii) positively gating for the high-density population in plotting FS vs. SS.

To unambiguously assess the expression of ChR2-EYFP in our samples, we subsampled each 30,000-point data set into 100 independent data sets. The log fluorescence (EYFP intensity) of each of these 100 subsets was then independently fit to a multi-component Gaussian mixture model that chose whether the data set was best fit by one or by more than one curve, using the Bayesian information criterion to generate an accurate statistical estimate of the distinct subpopulations best accounting for each set of observations.

Animals. Adult wild-type male and female transgenic parvalbumin-IRES-Cre[30] (Jax 008069), parvalbumin-2a-Cre[29] (Jax 012358), tyrosine hydroxylase–Cre (EMMA 00254) and somatostatin-Flp C57/BL6 mice were group housed up to four to a cage and kept on a reverse 12-h light/dark cycle with *ad libitum* food and water. Experimental protocols were approved by Stanford University IACUC and meet guidelines of the US National Institutes of Health guide for the Care and Use of Laboratory Animals. See the **Supplementary Note** for additional experimental animal information.

mRNA isolation and cDNA synthesis. HEK293FT cells at 90% confluence were transfected with endotoxin-free DNA using Lipofectamine 2000 (Invitrogen) following the manufacturer protocol. Five days post transfection, RNA extraction was performed using reagents from the RNeasy Mini Kit (Qiagen). Cells were disrupted with lysis buffer and homogenized using QiaShredder homogenizer columns. Combined first-strand cDNA/PCR using the SuperScript III One-Step RT-PCR System (Invitrogen) was performed with the following reaction conditions: 45 °C × 30 min, 94 °C × 2 min, 40 cycles of 94 °C × 15 s, 45 °C × 30 s, 68 °C × 1 min, ending with 68 °C × 5 min using various combinations of primers (F, forward; R, reverse) as follows. Exon/strand/sequence (5′–3′): 1/F/agtggctgctcacttgtcct; 2/R/gcacaatccaagacaaaagaag; 2/F/agctggacggcgacgtaaac; 3/R/aagtcgtgctgcttcatgtg. The PCR product was gel purified and sequenced to determine splice junctions.

Mutagenesis. Intron mutations were introduced using QuikChange Lightning II Mutagenesis Kit (Agilent) with the following primers. F (5′–3′) and R (5′–3′): ChR2 C417A, ctgagcaacctcacaggtacgtgtcgggg and ccccgacacgtacctgtgaggttgctcag; intron 1 C4A, caacctcaccggtaagtgtcggggttgc and gcaaccccgacacttaccggtgaggttg; intron 1 polypyrimidine tract, gtgcttatgactctatttctcttctctttaggcctgagcaacgacta and tagtcgttgctcaggcctaaagagaagagaaatagagtcataagcac.

Virus production. *AAV-2/5.* Adeno-associated virus (AAV) serotype 2/5 was produced by the University of North Carolina Chapel Hill Vector Core.

AAV-DJ. AAV-DJ serotype was produced by the Stanford Neuroscience Gene Vector and Virus Core. In brief, AAV-DJ[41] was produced by transfection of AAV 293 cells (Agilent) with three plasmids: an AAV vector expressing the recombinase-dependent construct, AAV helper plasmid (pHELPER; Agilent) and AAV rep-cap helper plasmid (pRC-DJ, gift from M. Kay, Stanford University). At 72 h post transfection, the cells were collected and lysed by a freeze-thaw procedure. Viral particles were then purified by an iodixanol step-gradient ultracentrifugation method. The iodixanol was diluted and the AAV was concentrated using a 100-kDa molecular mass–cutoff ultrafiltration device. Genomic titer was determined by quantitative PCR. Infectious titers were determined on HEK293 cells and/or primary neurons.

AAV-10. AAV-10 was packaged via pseudotyping in AAV-10 capsid proteins in the laboratory of C. Bass (University at Buffalo), using the standard triple-transfection technique.

Lentivirus. Lentivirus was prepared as described previously[42] using triple transfection of HEK293 cells with VSVG, pDelta and payload constructs. For rapid construct prototyping, small batches were made from single 225-cm^2 plates.

HSV. Long-term herpes simplex virus (LT-HSV) was created by modification of short-term HSV (ST-HSV) as follows: the polyadenylation (pA) signal changed from SV40 late pA to SV40 early pA, and the 692-bp WPRE[43] was added. LT-HSV vectors are available from the Massachusetts Institute of Technology Viral Gene Transfer Core.

Histology. Following virus injection, mice were transcardially perfused with 20 mL of ice-cold PBS followed by 20 mL of 4% paraformaldehyde (PFA). After an overnight postfix in PFA, brains were equilibrated in sterile 30% sucrose/PBS for at least 24 h. Tissue was sectioned at 40 µm using a frozen microtome, stained and mounted with PVA-DABCO (Sigma). Images were

doi:10.1038/nmeth.2996

obtained on a Leica confocal microscope using 5×, 40×, and 63× objectives. All secondary antibodies (Jackson ImmunoResearch) were used at 1:500. Primary antibodies were 2a (Millipore ABS31, rabbit, 1:500 dilution), parvalbumin (Sigma P3088, mouse, 1:500), somatostatin (Santa Cruz Sc-7819, goat, 1:500), tyrosine hydroxylase (Aves TYH, chicken, 1:500), streptavidin-350 (Invitrogen S-11249, 1:500).

***In vivo* optrode recordings.** *In vivo* recordings of recombinase-induced ChR2 expression in hippocampus were performed as described previously[44]. Clampex software was used for both recording signals and controlling the 473-nm (CrystaLaser) 100-mW solid-state laser diode source coupled to the optrode. Neuronal activity was evoked by 1.5 s of pulsed (10 Hz, 5-ms pulse width) 473-nm light.

Culture electrophysiology. Primary hippocampal neurons produced, plated, and transfected as above were identified for recording by fluorescent protein expression. Recordings were obtained in Tyrode's medium (in mM: 150 NaCl, 4 KCl, 2 $MgCl_2$, 2 $CaCl_2$, 10 D-glucose, 10 HEPES, adjusted to pH 7.35 with NaOH) supplemented with TTX (Tocris, 1 μM), APV (Tocris, 10 μM), and/or CNQX (Tocris, 25 μM) as indicated with a standard internal solution (in mM: 130 K-gluconate, 10 KCl, 10 HEPES, 10 EGTA, 2 $MgCl_2$, to pH 7.3 with KOH) in 3- to 5-MΩ glass pipettes. Filtered light from a xenon lamp (DG-4 Sutter Instruments) was coupled to the fluorescence port of the microscope (Leica DM-LFSA). The ChR2 stimulation filter (473 nm, Semrock) had an approximately 20-nm bandwidth.

Slice electrophysiology. Coronal slices (300 μm) from mice previously injected with virus were prepared after intracardial perfusion with ice-cold, sucrose-containing artificial cerebrospinal fluid (ACSF; in mM): 85 NaCl, 75 sucrose, 2.5 KCl, 25 glucose, 1.25 NaH_2PO_4, 4 $MgCl_2$, 0.5 $CaCl_2$ and 24 $NaHCO_3$. Slices were incubated for 1 h at 32–34 °C and then transferred to an oxygenated standard ACSF solution at room temperature (in mM): 123 NaCl, 3 KCl, 26 $NaHCO_3$, 2 $CaCl_2$, 1 $MgCl_2$, 1.25 NaH_2PO_4 and 11 glucose, with synaptic transmission blockers D-2-amino-5-phosphonovaleric acid (APV; 25 μM), 2,3-dihydroxy-6-nitro-7-sulfamoyl-benzo[f]quinoxaline-2,3-dione (NBQX; 10 μM) and gabazine (10 μM). Electrophysiological recordings were performed at 32–34 °C. Slices were visualized with an upright microscope (BX61WI, Olympus) equipped with a 40× water-immersion objective and infrared differential interference contrast (IR-DIC) optics. Individual neuron recordings were obtained after identifying fluorescent protein expression without interruption of ACSF perfusion. Filtered light from a Spectra X Light engine (Lumencor) was coupled to the fluorescence port of the microscope and used to both view fluorescence and deliver light pulses for opsin activation. Power density of the blue light (475/28 nm) was 5 mW/mm^2, measured with a power meter (Thorlabs). Whole-cell recordings were obtained with patch pipettes pulled from borosilicate glass capillaries (Sutter Instruments) with a horizontal puller (P-2000, Sutter Instruments) and contained the following internal solution (in mM): 125 K-gluconate, 10 KCl, 10 HEPES, 4 Mg_3-ATP, 0.3 Na-GTP, 10 phosphocreatine, 1 EGTA, 8 biocytin. 1 μM tetrodotoxin was added to the external recording solution when necessary to eliminate escape spikes for peak photocurrent measurements. Recordings were made using a MultiClamp700B amplifier (Molecular Devices). Signals were filtered at 4 kHz and digitized at 10 kHz with a Digidata 1440A analog-digital interface (Molecular Devices). pClamp10.3 software (Molecular Devices) was used to record and analyze data. Peak and steady-state photocurrents were measured from a 1-s light pulse in voltage-clamp mode. Series resistances were carefully monitored, and recordings were not used if the series resistance changed by a large magnitude (by >20%) or reached 25 MΩ. Input resistance and capacitance were both calculated from the response to 10-mV voltage steps in voltage clamp, using steady-state current amplitude and recovery from the capacitive transient, respectively.

Slice histology. 300-μm acute slices used in electrophysiology recordings with biocytin-filled recording pipettes were prepared in a two-step process. Slices were first processed for immunohistochemistry by postfixing in 4% PFA with 0.2% picric acid in 0.1 M phosphate buffer (in mM: 80 Na_2HPO_4, 20 NaH_2PO_4) for at least 1 d following recording, washed in 0.1 M phosphate buffer (PB) and incubated overnight at 4 °C with primary antibodies diluted in 0.05 M TBS (in mM: 42 Trizma HCl, 8 Trizma base, 154 NaCl) with 0.5% Triton X-100. The next day, slices were washed in 0.1 M TBS, incubated in secondary at room temperature for 3 h, washed in 0.1 M PB and mounted using Vectashield (Vector Laboratories). After imaging, slices were processed for bright-field morphological analysis.

For morphological analysis of axonal and dendritic arbors, slices were unmounted; washed in 0.1 M PB; treated with 1% H_2O_2 to extinguish endogenous peroxidases; washed again; treated with 50%, 70%, and 50% EtOH steps; washed; and processed to form avidin-DH/biotin complexes (Vectastain ABC kit, Vector Laboratories) in 0.05 M TBS with 0.5% Triton X-100 overnight at 4 °C. The next day, after washing in 0.1 M PB, slices were reacted with 3,3′-diaminobenzidine tetrahydrochloride (0.015%, DAB substrate kit for peroxidase, Vector Laboratories), washed, dehydrated, cleared with Citrisolv (Fisherbrand) and mounted (DPX, Electron Microscopy Sciences). Morphology was resolved by examining shape and location of cell body, dendrites and axon; reconstructions were rendered with StereoInvestigator (MBF) and Photoshop (Adobe).

40. Brunak, S., Engelbrecht, J. & Knudsen, S. Prediction of human mRNA donor and acceptor sites from the DNA sequence. *J. Mol. Biol.* **220**, 49–65 (1991).
41. Grimm, D. *et al.* *In vitro* and *in vivo* gene therapy vector evolution via multispecies interbreeding and retargeting of adeno-associated viruses. *J. Virol.* **82**, 5887–5911 (2008).
42. Zhang, F. *et al.* Optogenetic interrogation of neural circuits: technology for probing mammalian brain structures. *Nat. Protoc.* **5**, 439–456 (2010).
43. Donello, J.E., Loeb, J.E. & Hope, T.J. Woodchuck hepatitis virus contains a tripartite posttranscriptional regulatory element. *J. Virol.* **72**, 5085–5092 (1998).
44. Gradinaru, V. *et al.* Targeting and readout strategies for fast optical neural control *in vitro* and *in vivo*. *J. Neurosci.* **27**, 14231–14238 (2007).